

Adaptive Trajectory Estimation with Power Limited Steering Model under Perturbation Compensation

Wei-Peng Li¹, Xiao-Gang Yang², Rui-Tao Lu³

Abstract: Trajectory estimation under regional correlations is applied in numerous tasks like dynamic path planning, navigation and tracking. Many previous works get impressive results in the strictly controlled condition with accurate prior statistics and specific dynamic model for certain object. While in a more challenging situation without specific dynamic model and accurate prior statistics, the performance of these methods significantly declines. To estimate the trajectory without specific dynamic model, we propose a general model called the power-limited steering model (PLS), which is a natural combination of instantaneous power and instantaneous angular velocity. As a nonlinear model it needs less parameter to describe the switching of states compared with linear Markov process model. Then we derive the corresponding form in discrete time and compensate the nonlinear effect of perturbation with renormalization group. To overcome the biased prior statistics, the observations drift and linear growing computation in trajectory estimation, we propose the adaptive trajectory estimation (AdaTE) where the online updated statistics and the adaptive truncation time is applied. The experiment of typical trajectory estimation demonstrates that compared with EKF and UKF, AdaTE is more robust to the biased prior statistics and observation drift. Another task shows that with slight modification, AdaTE can be used in path planning that needs obstacle avoidance. Finally, we exhibit its potential application on trajectory optimization in visual tracking.

Keywords: adaptive trajectory estimation, general dynamic model, biased prior statistics, perturbation compensation

I. INTRODUCTION

Trajectory estimation plays a critical role from industrial appliances to research areas. It is widely used in numerous tasks like dynamic path planning [31], navigation, tracking [22] and simultaneous localization and mapping (SLAM) [32][33][34]. Successful trajectory estimation depends on three key aspects: effective dynamic model, precise measurement model, and robust estimation algorithm. Many previous works [13][14][15][16] have got impressive results under the strictly controlled condition, where an precise dynamic model of object, a precise measurement model, and some prior statistics can be obtained. However, these methods may be infeasible in a more challenging and common situation, where dynamic model and prior statistics are unobtainable or at least inaccurate for some uncontrollable factors. Moreover, some sensors may experience observation drift. It will lead to serious biased estimation if there is no correction.

To estimate the trajectory of object without specific dynamic model, many previous works focus on creating general dynamic models for maneuvering object. A large category of dynamic models is regarding the input or the control as a random variable. These includes some famous models like wiener-process acceleration model [6], Markov process models such as Singer model [7], and semi-Markov jump process models [8]. To accommodate a variety of states, many of these work committed to modeling the switching process between typical states, and they got excellent predictions when all of the quantized levels and corresponding probabilities are well assigned. But in practice, these models face two challenges when they are applied to maneuvering object. Firstly, the Markov jump process relies on the switching probability between quantized levels, while both the quantized levels and their conditional probability are hard to assign without abundant prior information. Secondly, most of these models assume the movements in orthogonal directions are uncoupled with each other, which will weaken the ability of trajectory prediction in many cases like making a turn. Besides, these dynamic models are linear model of the state. This may lose some important characters of nonlinear models, like multi-equilibrium states.

To overcome the major difficulties and design a better dynamic model, we learn from the previous works and propose the power-limited steering model (PLS). It is a nonlinear model of state based on a natural combination of instantaneous power theory and instantaneous angular velocity theory from Newtonian mechanics. Compared with constant mean acceleration model [9], it overcomes the infinite velocity problem in prediction with the joint action of power and damping. Compared with Markov process models, the strong nonlinearity make it only needs few prior parameters to describe the typical states.

This work was supported in part by the National Natural Science Foundation of China No.61806209 and Open Foundation of Shaanxi Key Laboratory of Integrated and Intelligent Navigation SKLIIN-20180103.

¹ High-tech Institute of Xi'an, Email: williamli_pro@163.com.

² High-tech Institute of Xi'an, Email: doctoryxg@163.com.

³ Corresponding author. High-tech Institute of Xi'an, Email: lrt19880220@163.com.

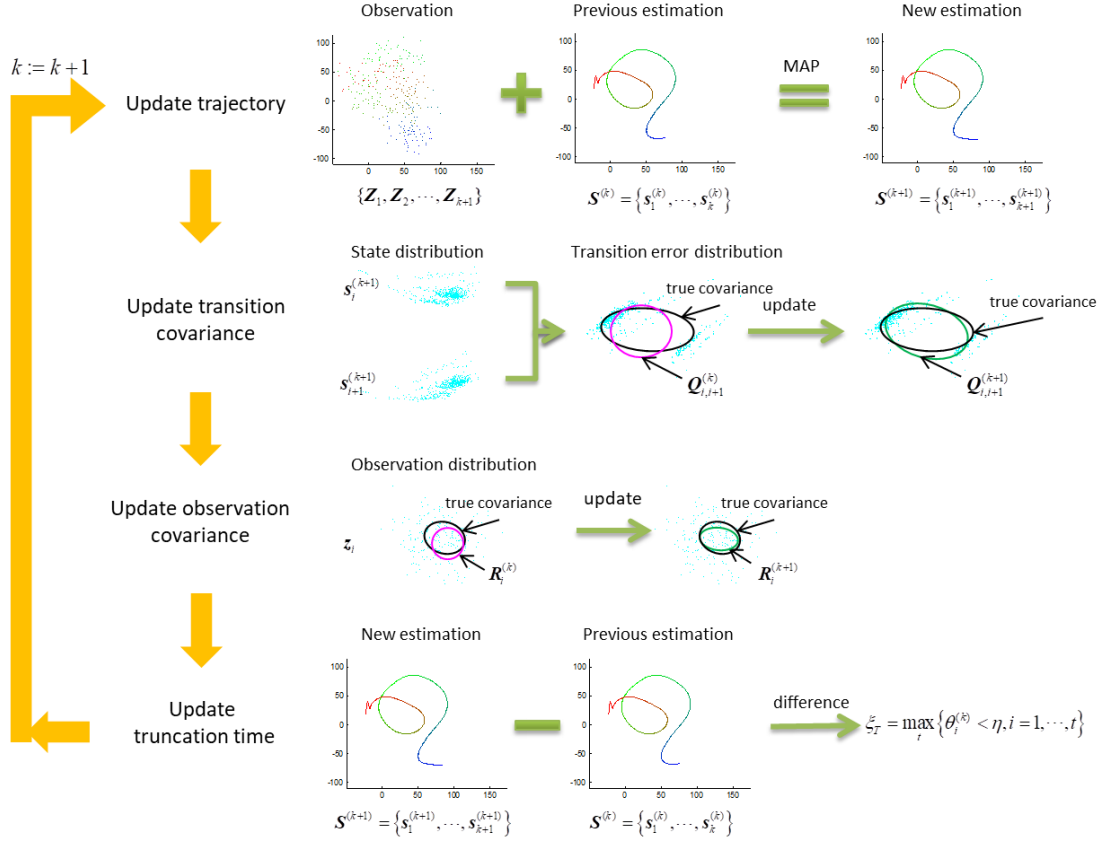


Fig 1. The process of adaptive trajectory estimation algorithm. The first step is updating the trajectory based on the observations and previous estimation with sparse MAP. The second step is updating the transition covariance of different times with a transition error. The third step is updating the observation covariance based on analysis of the observation error. Finally, the truncation time which confines the range to be updated will be worked out based on the difference between previous and updated trajectory.

To estimate the trajectory with precise solving algorithm, various approaches have been developed. One famous category is the Kalman filter [1][2] and Kalman smoother [13][16], which was designed for optimal sequential estimation of linear models. To expand the application to nonlinear models, the extended Kalman filter (EKF) and the Unscented Kalman Filter (UKF) [1][2] has been developed. But these classical filters have two shortages in common: (1) they are sensitive to the model error and seriously depend on prior statistics; (2) they use fixed and zeros centered noise model, which leads to the fragility to the observation drift. To overcome these problems, some specifically designed methods have been proposed, including the eXogenous Kalman Filter (XKF) [25] which is globally stable to nonlinear observer, the maximum correntropy Kalman filter (MCKF) [26] which is robust to large outlier observations, and the Robust Kalman Filtering (RKF) [27] which is robust to the model error. Each of these methods tries to solve a certain problem, but none of them can overcome all these difficulties in a single framework. Another famous filtering approach is particle filter [17][18][19][20]. Through the resampling strategy [19], the particle state distribution approximates the real distribution. Compared with Kalman filters, it is much more robust to the biased prior statistics. However, because of the huge computation for updating a massive number of trajectory particles, it is difficult to apply in real-time estimation.

Different from the filtering approaches, the optimization approaches can produce globally consistent result. A representative illustration is the graph optimization designed to optimize the trajectory for SLAM task. However, the basic form of this technique is sensitive to dynamic model and prior statistics. If strongly nonlinear models are invoked with biased prior statistics, wrong results and divergence may occur [3][4]. Besides, in optimization framework, sparse Cholesky factorization is usually used to accelerate the calculation [3]. But directly applying it in a task with only regional correlations would bring a lot of unnecessary computations.

This paper mainly focuses on the trajectory estimation under regional correlations. And we propose a specifically designed optimization method, called the adaptive trajectory estimation algorithm (AdaTE) based on the PLS. The process is plotted in Fig 1. Firstly, the trajectory is updated based on the previous estimation and corresponding statistics. Next, the state transition error is estimated, and the transition covariance is updated online. Then, the observation covariance is updated based on the difference between the real observation and the estimated one from trajectory. Finally, the truncation time which confines the

range to be updated is worked out based on the difference between previous and updated trajectory. All of these carefully designed steps are meaningful. The adaptation of transition covariance improves the robust to both model error and prior statistics. The correction of observation covariance improves the resistance to the observation drift. Furthermore, the truncation time ensures the update is confined to necessary part, which avoids the linear improvement of calculation.

The remainder of this paper will be mentioned as follows. Section II familiarizes the reader with related researches in dynamic model and trajectory estimation algorithm. Section III presents the power limited steering model (PLS) and derives the corresponding discrete-time form. Section IV describes the detail of adaptive trajectory estimation algorithm. Section V introduces three experiments in different tasks: trajectory estimation with 3D observations, 3D path planning and trajectory estimation for visual tracking. The paper is summarized in Section VI.

II. RELATED WORKS

Dynamic model and estimation algorithm are two key factors for trajectory estimation. In this section, we firstly introduce some subclass of dynamic model, their representative members, and their relationship and difference with PLS model. Then we talk about the estimation algorithm and make a contrast of filtering methods with optimization methods.

A. Dynamic model

In most cases, the control of maneuvering object is unknown to the observer. To design a dynamic model for maneuvering object, a popular alternative is to describe the movement as a stochastic process with random control. These models can be classified into three subclasses: white noise models, Markov process models and Semi-Markov process models. And most of them assume the movements in orthogonal directions are uncoupled with each other.

One of the simplest and representative dynamic models is the Wiener-process acceleration model [6], where acceleration is assumed to obey the Wiener process. It is the ancestor of many following constant acceleration (CA) models.

Lets \mathbf{x} , \mathbf{v} and \mathbf{a} be the position, velocity and acceleration of the object, and the state vector is

$$\mathbf{s} = \begin{bmatrix} \mathbf{x} \\ \mathbf{v} \\ \mathbf{a} \end{bmatrix} \quad (1)$$

The Wiener-process acceleration model is defined as

$$\dot{\mathbf{s}} = \mathbf{A}\mathbf{s} + \mathbf{u} \quad (2)$$

where \mathbf{u} is the control. It is an independent process (white noise) of acceleration with power spectral density \mathbf{D} . \mathbf{A} is the state transition matrix,

$$\mathbf{A} = \begin{bmatrix} \mathbf{0} & \mathbf{I} & \mathbf{0} \\ \mathbf{0} & \mathbf{0} & \mathbf{I} \\ \mathbf{0} & \mathbf{0} & \mathbf{0} \end{bmatrix} \quad (3)$$

where \mathbf{I} is the identity matrix.

Based on the antitype of Wiener-process, many following models have been proposed, such as the polynomial models, the Singer model [7], “current” model and semi-Markov jump process model [8]. Their improvement mainly focuses on the distribution of random vector, such as quantized levels of expectations,

$$\mathbf{u}(t) = \sum_{i=1}^n \bar{\mathbf{a}}_i P\{\mathbf{u}(t) = \bar{\mathbf{a}}_i | \mathbf{z}(s), s < t\} + \tilde{\mathbf{a}} \quad (4)$$

where $\bar{\mathbf{a}}_i$ is the quantized expectation of acceleration, $\tilde{\mathbf{a}}$ is the zero-mean random vector, and $\mathbf{z}(s), s < t$ is all of the observations before time t .

Or modify the state transition matrix, such as adding the damping term

$$\dot{\mathbf{a}} = -\beta\mathbf{v} + \mathbf{u} \quad (5)$$

where β is the damping factor.

Whatever they have changed, these dynamic models are linear model of the state. That means if they want to describe different typical movements in a model, they have to define a lot of quantized levels and corresponding conditional probability based on abundant prior information. A typical illustration is the quantized expectations of acceleration $\bar{\mathbf{a}}_i, i = 1, 2, \dots, n$ defined in (4).

Another impressive work is the generative model for maneuvering target tracking (GMTM) [10], where the motive force is divided into the axial force and centripetal force to describe axial acceleration and angular velocity based on Newton mechanics. In general, it is a nonlinear model of state vector.

Inspired by GMTM [10], we propose a nonlinear dynamic model, the power-limited steering model (PLS). Its main innovation is the combination of instantaneous power theory and instantaneous angular velocity theory from Newton mechanics. What should be explained is that, we choose the power instead of the force as the dynamic source simply because the movement of real object is directly driven by power. On the one hand, because PLS is a nonlinear model, it needs fewer prior parameters to describe the typical states compared with Markov process models. On the other hand, the nonlinearity of PLS leads to the extra difficulty in deriving corresponding discrete time model.

B. Estimation algorithm

The estimation algorithm can be conventionally separated into two categories: filtering approaches and optimization approaches. Normally, filtering approaches result in the expectation of the states at each time under certain distribution, while optimization approaches estimate a trajectory with maximum global probability. The filtering approaches have been widely used in previous works because they were believed to require fewer computations compared with optimization approaches. Until the optimization framework was found to have sparse associations, it starts to be applied widely.

One kind of the well-known filtering approaches is the Kalman Filter family. The members include Kalman Filter (KF), extended Kalman filter (EKF), Unscented Kalman Filter (UKF) [1][2], Cubature Kalman Filters (CKF) [23][24], and some recent developed methods such as eXogenous Kalman Filter (XKF) [25] and the Maximum Correntropy Kalman filter (MCKF) [26]. For the real-time state estimation, they only execute a forward propagation:

$$E[s_k | \mathcal{Z}_k] = \int \left[\int \frac{P(\mathbf{Z}_k | s_k) P(s_k | s_{k-1}, \mathcal{Z}_{k-1})}{P(\mathbf{Z}_k)} ds_{k-1} \right] s_k ds_k \quad (6)$$

where $s_i, i \in \{1, \dots, k\}$ is the state at time i , \mathcal{Z}_k is the observations at time k which might contain several independent observations, and $\mathcal{Z}_k = \{\mathbf{Z}_1, \dots, \mathbf{Z}_k\}$ is the set of observations from time 1 to time k .

While in trajectory estimation, they have to correct the previous states in an inverse time order:

$$E[s_i | \mathcal{Z}_k] = \int \left[\int P(s_{i+1} | s_i, \mathcal{Z}_k) P(s_i | \mathcal{Z}_{k-1}) ds_{i+1} \right] s_i ds_i, i = k-1, \dots, 1 \quad (7)$$

Because the trajectory is estimated as a set of expectations at different moments, the result is not the trajectory with the highest probability but rather a compromise. In detail, if there is a precise dynamic model and accurate prior statistics, it would be easy to obtain an accurate trajectory. However, for some objects, we are difficult to obtain a precise dynamic model and prior statistics. For example, if the prior statistics indicate that the noise of observation is zero-mean while it has drift in fact, there will be systematic deviation in result. Besides, how to set the truncation time to limit the range of trajectory to be updated is another problem for the filtering approaches. Although some researches already worked on this issue, like restricted memory filtering, they still left some problem such as how to adjust the length of memory online.

Different from the filtering approaches, the optimization approaches, such as graph optimization [28][29][30] for SLAM [32][33][34], can be mentioned as finding the trajectory with the highest probability from observations:

$$\mathcal{S}_k = \arg \max P(\mathcal{S}_k | \mathcal{Z}_k) \quad (8)$$

where $\mathcal{S}_k = \{s_1, \dots, s_k\}$ is a set of states from time 1 to time k .

For a linear model with a simple distribution, (8) has an analytic solution. For nonlinear model or complex distribution that do not have analytic solutions, numerical solutions can be worked out through the Newton-Raphson, BFGS [35] or the gradient descent algorithm [36].

In general, the optimization approaches should have sequential iterative algorithm for online estimation. Because the last estimation is optimized based on the best estimation in the previous time, and the initial estimation has a smooth and small solution space, the result of sequential iteration will be always close to the global optimum. It should be noticed that, if a new observation is inconsistent with the previous estimation, the optimization algorithm often needs extra time to correct the trajectory. Otherwise if we choose to believe the previous estimation, to what extent and on what time we should correct the trajectory? Moreover, sparse Cholesky factorization is usually used to accelerate the optimization process [3]. It is designed for optimization with global correlations, but directly applying it in a task only with regional correlations (such as visual tracking) would bring a lot of unnecessary computation.

Both of the listed filtering approaches and optimization approaches have a common problem: they urgently depend on prior statistics. If the prior statistics are incorrect, the result of these algorithms may have extra error. Moreover, if the dynamic model is nonlinear, such as the PLS in this paper, this error may be magnified.

To overcome the shortages of listed algorithms and integrate their advantages, the newly designed AdaTE should have following abilities: (a) be insensitive to prior statistics, (b) can find out the observation outliers and correct their statistics, (c) adjust the truncation time based on the estimation fluctuation.

III. POWER LIMITED STEERING MODEL

In many dynamics models, the movements in orthogonal directions are assumed to be uncoupled with each other [11][12]. But in fact the opposite is true, and the assumption will weaken the ability of trajectory prediction in many cases like making a turn. We learn from the previous works and propose the power-limited steering model (PLS). It is a nonlinear model of state based on a natural combination of instantaneous power theory and instantaneous angular velocity theory from Newtonian mechanics. Compared with constant mean acceleration model [9], the PLS overcomes the infinite velocity problem in prediction with the joint action of power and resistance. Compared with Markov process models, the strong nonlinearity of PLS enables that it only needs few prior parameters to describe the typical states. Firstly, we introduce the PLS in continuous time, then derive its corresponding form in discrete time.

A. Power-limited steering model in continuous time

The movement of an object can be decomposed into the axial and transverse direction. According to Newtonian mechanics, if the object is driven by power P and receives resistance β and damping α , the axial acceleration is:

$$\mathbf{a}_A = -\alpha \mathbf{v} - \beta \frac{\mathbf{v}}{|\mathbf{v}|} + \frac{P\mathbf{v}}{m|\mathbf{v}|^2} \quad (9)$$

where m is the mass of object.

Setting $p = \frac{P}{m}$ be the power-mass ratio (specific power), which represents the power assigned to a unit mass in physics, (9) can be rewritten as

$$\mathbf{a}_A = -\alpha \mathbf{v} - \beta \frac{\mathbf{v}}{|\mathbf{v}|} + p \frac{\mathbf{v}}{|\mathbf{v}|^2} \quad (10)$$

It is easy to find that when the power is a constant positive number, the velocity will be asymptotically stabilized to $\frac{-\beta + \sqrt{\beta^2 + 4\alpha p}}{2\alpha}$.

Similar to (10), the acceleration in the transverse direction is given by

$$\mathbf{a}_T = \mathbf{c}_T \times \mathbf{v} = [\mathbf{c}_T]_{\times} \mathbf{v} \quad (11)$$

which is orthogonal to \mathbf{v} , and the vector \mathbf{c}_T is the instantaneous angular velocity.

The variation of p and \mathbf{c}_T should be smooth, so we set $\dot{p} = u_A$ and $\dot{\mathbf{c}}_T = \mathbf{u}_T$ as the axial and transverse controls. As a maneuvering object, the controls u_A and \mathbf{u}_T have high randomness and low temporal correlation. So they are assumed to be time-independent and zero-mean random pulse obeying the normal distribution,

$$u_A(t) \sim \mathcal{N}\{0, \delta_t(s) D_A\} \quad (12)$$

$$\mathbf{u}_T(t) \sim \mathcal{N}\{\mathbf{0}, \delta_t(s) \mathbf{D}_T\} \quad (13)$$

Where $\delta_t(s)$ is the delta function, D_A and \mathbf{D}_T are the power spectral density of u_A and \mathbf{u}_T .

Combining the axial and the transverse movement, the power-limited steering model in continuous time satisfies

$$\begin{cases} \dot{\mathbf{x}} = \mathbf{v} \\ \dot{\mathbf{v}} = -\alpha \mathbf{v} - \beta \frac{\mathbf{v}}{|\mathbf{v}|} + p \frac{\mathbf{v}}{|\mathbf{v}|^2} - [\mathbf{v}]_{\times} \mathbf{c}_T \\ \dot{p} = u_A \\ \dot{\mathbf{c}}_T = \mathbf{u}_T \end{cases} \quad (14)$$

Next we will discuss the solution of (14).

B. The short-term evolution of velocity

Noticing (14) is a nonlinear stochastic function, where u_A , \mathbf{u}_T will cause the perturbation of p and \mathbf{c}_T , which is hard to be solved directly. To simplify the problem, we will solve the velocity ignoring the perturbation of p and \mathbf{c}_T at first, and then compensate the effect of perturbation.

For differential equation (14), the axial and transverse velocity can be separated into two differential equations:

$$\begin{cases} |\mathbf{v}| \frac{d|\mathbf{v}|}{dt} = p - \alpha |\mathbf{v}|^2 - \beta |\mathbf{v}| \\ \dot{p} = u_A \end{cases} \quad (15)$$

and

$$\begin{cases} \frac{d}{dt} \frac{\mathbf{v}}{|\mathbf{v}|} = [\mathbf{c}_T]_{\times} \frac{\mathbf{v}}{|\mathbf{v}|} \\ \dot{\mathbf{c}}_T = \mathbf{u}_T \end{cases} \quad (16)$$

where u_A and \mathbf{u}_T obeys (12) and (13).

Firstly, ignoring the perturbations of p and \mathbf{c}_T during a short time τ , we can solve the biased prediction of velocity $\hat{\mathbf{v}}(t + \tau)$ from appendix A,

$$\begin{cases} \left(\frac{|\hat{\mathbf{v}}(t + \tau)| + \varsigma_1}{|\mathbf{v}(t)| + \varsigma_1} \right)^{\varsigma_1} \left| \frac{|\hat{\mathbf{v}}(t + \tau)| + \varsigma_2}{|\mathbf{v}(t)| + \varsigma_2} \right|^{-\varsigma_2} = e^{-\gamma\tau} \\ \frac{\hat{\mathbf{v}}(t + \tau)}{|\hat{\mathbf{v}}(t + \tau)|} = \exp(\tau [\mathbf{c}_T(t)]_{\times}) \frac{\mathbf{v}(t)}{|\mathbf{v}(t)|} \end{cases} \quad (17)$$

where ς_1 and ς_2 are defined in (54), and γ is defined in (55).

It is hard to solve the analytical solution of $|\hat{\mathbf{v}}(t + \tau)|$ from (17) directly, but we can quickly work out the arithmetic solution from (17) with Newton-Raphson method.

After the estimation of $\hat{\mathbf{v}}(t + \tau)$ under perturbation ignorance, the effect of perturbation should be compensated into estimated velocity. Based on the renormalization group, the compensation of axial velocity can be derived from appendix B,

$$\Delta v(t, t + \tau) = -\frac{v_0 D_A}{2\mu(t)} \left[\tau - \frac{2v_0^2}{\mu(t)} \log \frac{v_0^2 + \tau\mu(t)}{v_0^2} + \frac{v_0^2 \tau}{v_0^2 + \tau\mu(t)} \right] \quad (18)$$

where $\mu(t) = p(t) - v_0(\alpha v_0 + \beta)$, $v_0 = |\mathbf{v}(t)|$.

Combining (17) and (18), the corrected prediction of axial velocity is,

$$|\bar{\mathbf{v}}(t + \tau)| = |\hat{\mathbf{v}}(t + \tau)| + \Delta v(t, t + \tau) \quad (19)$$

And the direction of velocity satisfies,

$$\frac{\bar{\mathbf{v}}(t + \tau)}{|\bar{\mathbf{v}}(t + \tau)|} = \exp(\tau [\mathbf{c}_T(t)]_{\times}) \frac{\mathbf{v}(t)}{|\mathbf{v}(t)|} \quad (20)$$

C. PLS model in discrete time

To match the requirement of the optimization algorithm in next section, the state transition should be written in a linear form

$$\mathbf{s}(t + \tau) = \boldsymbol{\Phi}(t, t + \tau) \mathbf{s}(t) + \boldsymbol{\varepsilon}(t, t + \tau) \quad (21)$$

where $\mathbf{s} = [\mathbf{x}^T \ \mathbf{v}^T \ p \ \mathbf{c}_T^T]^T$ is the state vector, $\boldsymbol{\Phi}(t, t + \tau)$ is the state transition matrix from t to $t + \tau$, $\boldsymbol{\varepsilon}(t, t + \tau)$ is the vector of transition error which satisfies,

$$\boldsymbol{\varepsilon}(t, t + \tau) = \int_0^\tau \boldsymbol{\Phi}(t + s, t + \tau) \mathbf{u}(t + s) ds \quad (22)$$

and $\mathbf{u} = [\mathbf{0} \ \mathbf{0} \ u_A^T \ \mathbf{u}_T^T]^T$ is the control vector where u_A and \mathbf{u}_T satisfies (12) and (13).

Because the transition matrix is the foundation of calculating the transition error $\boldsymbol{\varepsilon}(t, t + \tau)$, we will discuss the transition matrix at first, and analyze the error later.

According to (17)-(20), the velocity at time $t + \tau$ can be mentioned as,

$$\mathbf{v}(t + \tau) = \bar{\mathbf{v}}(t + \tau) + \delta \mathbf{v}(t + \tau) = \exp(\tau [\mathbf{c}_T(t)]_{\times}) \frac{|\bar{\mathbf{v}}(t + \tau)|}{|\mathbf{v}(t)|} \mathbf{v}(t) + \delta \mathbf{v}(t, t + \tau) \quad (23)$$

where $\delta \mathbf{v}(t, t + \tau)$ is the error of velocity transition.

Combining (17) and (19), the axial velocity can be decomposed as,

$$|\bar{\mathbf{v}}(t+\tau)| = (|\mathbf{v}(t)| + \varsigma_1) e^{-\lambda\tau} g_{(t,t+\tau)} - \varsigma_1 + \Delta v(t, t+\tau) \quad (24)$$

where

$$\begin{cases} g_{(t,t+\tau)} = \frac{|\hat{\mathbf{v}}(t+\tau)| + \varsigma_2}{|\mathbf{v}(t)| + \varsigma_2} \left| \frac{\varsigma_2}{\varsigma_1} \right| \\ \lambda = \frac{\gamma}{\varsigma_1} \end{cases} \quad (25)$$

Plug (24) into (23), the $\mathbf{v}(t+\tau)$ satisfies,

$$\mathbf{v}(t+\tau) = \frac{(|\mathbf{v}(t)| + \varsigma_1) e^{-\lambda\tau} g_{(t,t+\tau)} - \varsigma_1 + \Delta v(t, t+\tau)}{|\mathbf{v}(t)|} \exp(\tau [\mathbf{c}_T(t)]_{\times}) \mathbf{v}(t) + \delta \mathbf{v}(t+\tau) \quad (26)$$

After the approximation,

$$\mathbf{v}(t+\tau) \approx \left(e^{-\lambda\tau} g_{(t,t+\tau)} + \frac{\Delta v(t, t+\tau)}{|\mathbf{v}(t)|} \right) \mathbf{v}(t) + h_{(t,t+\tau)} (1 - e^{-\lambda\tau} g_{(t,t+\tau)}) \frac{\mathbf{v}(t)}{|\mathbf{v}(t)|} p(t) - \tau \varphi_{(t,t+\tau)} [\mathbf{v}(t)]_{\times} \mathbf{c}_T(t) + \delta \mathbf{v}(t+\tau) \quad (27)$$

where

$$\begin{cases} h_{(t,t+\tau)} = \frac{2}{\beta - \gamma} \\ \varphi_{(t,t+\tau)} = e^{-\lambda\tau} g_{(t,t+\tau)} + \frac{\Delta v(t, t+\tau)}{|\mathbf{v}(t)|} + \frac{h_{(t,t+\tau)} p(t)}{|\mathbf{v}(t)|} (1 - e^{-\lambda\tau} g_{(t,t+\tau)}) \end{cases} \quad (28)$$

By this way, the velocity $\mathbf{v}(t+\tau)$ is written as a linear form of $\mathbf{v}(t)$, $p(t)$ and $\mathbf{c}_T(t)$. And the transition matrix can be derived with the velocity from (27):

$$\begin{aligned} \Phi(t, t+\tau) &\approx \\ &\begin{bmatrix} \mathbf{I} & \Phi_{12}(t, t+\tau) & \Phi_{13}(t, t+\tau) & \Phi_{14}(t, t+\tau) \\ \mathbf{0} & \Phi_{22}(t, t+\tau) & \Phi_{23}(t, t+\tau) & \Phi_{24}(t, t+\tau) \\ \mathbf{0} & \mathbf{0} & 1 & \mathbf{0} \\ \mathbf{0} & \mathbf{0} & \mathbf{0} & \mathbf{I} \end{bmatrix} \end{aligned} \quad (29)$$

where

$$\begin{cases} \Phi_{12}(t, t+\tau) = \tau \left(0.5 + 0.5 e^{-\lambda\tau} g_{(t,t+\tau)} + \frac{\Delta v(t, t+\tau)}{2|\mathbf{v}(t)|} \right) \mathbf{I} \\ \Phi_{13}(t, t+\tau) = \tau (0.5 - 0.5 e^{-\lambda\tau} g_{(t,t+\tau)}) \frac{h_{(t,t+\tau)} \mathbf{v}^*(t)}{|\mathbf{v}^*(t)|} \\ \Phi_{14}(t, t+\tau) = -\frac{1}{2} \tau^2 \varphi_{(t,t+\tau)} [\mathbf{v}^*(t)]_{\times} \\ \Phi_{22}(t, t+\tau) = \left(e^{-\lambda\tau} g_{(t,t+\tau)} + \frac{\Delta v(t, t+\tau)}{|\mathbf{v}(t)|} \right) \mathbf{I} \\ \Phi_{23}(t, t+\tau) = (1 - e^{-\lambda\tau} g_{(t,t+\tau)}) \frac{h_{(t,t+\tau)} \mathbf{v}^*(t)}{|\mathbf{v}^*(t)|} \\ \Phi_{24}(t, t+\tau) = -\tau \varphi_{(t,t+\tau)} [\mathbf{v}^*(t)]_{\times} \end{cases} \quad (30)$$

After getting the transition matrix, we analyze the transition error defined in (22).

Because the expectation of velocity perturbation have been compensated in (19), $\boldsymbol{\varepsilon}(t, t+\tau)$ will be a zero-mean random vector. Thus we only need to consider the transition covariance,

$$\mathbf{Q}(t, t + \tau) = \text{Cov}[\boldsymbol{\varepsilon}(t, t + \tau)] = \int_t^{t+\tau} \boldsymbol{\Phi}(t, s) \mathbf{D}_u \boldsymbol{\Phi}^T(t, s) ds \quad (31)$$

where \mathbf{D}_u is the power spectral density of \mathbf{u} , which satisfies,

$$\mathbf{D}_u = \int_t^{t+\tau} \text{E}[\mathbf{u}(s_1) \mathbf{u}^T(s_2)] ds_1 = \text{diag}\{0 \quad 0 \quad \mathbf{D}_A \quad \mathbf{D}_T\} \quad (32)$$

Because the time interval τ is small, the higher-order terms of $\mathbf{Q}(t, t + \tau)$ can be ignored. Then the approximated $\mathbf{Q}(t, t + \tau)$ can be calculated from appendix C.

Let $\boldsymbol{\Phi}_{k,k+1} = \boldsymbol{\Phi}(t_k, t_{k+1})$, and $\mathbf{Q}_{k,k+1} = \mathbf{Q}(t_k, t_{k+1})$, the state transition in discrete time can be written in a linear form,

$$\mathbf{s}_{k+1} = \boldsymbol{\Phi}_{k,k+1} \mathbf{s}_k + \boldsymbol{\varepsilon}_{k,k+1} \quad (33)$$

where $\boldsymbol{\varepsilon}_{k,k+1} \sim \mathcal{N}\{\mathbf{0}, \mathbf{Q}_{k,k+1}\}$.

It should be noted that although the $\boldsymbol{\Phi}_{k,k+1}$ implicitly include the state vector, the estimation algorithm based on this model still converges, and it can be verified by the experiments in section V.

IV. ADAPTIVE TRAJECTORY ESTIMATION

As a maneuvering object, the prior statistics are inaccurate. This will lead to the extra error of the algorithms which urgently relying on the prior statistics. While the PLS is a nonlinear model, the error may be magnified. Combining with other difficulties, such as the observations drift, the adaptive trajectory estimation algorithm should have following abilities: (a) be insensitive to prior statistics, (b) can find out the outliers and correct their statistics, (c) adjust the truncation time based on the estimation fluctuation. According to these principles, we design the AdaTE for online trajectory estimation. In general, it contains 4 steps: (a) updating the trajectory with sparse maximum a posterior estimation (sparse MAP); (b) updating the transition covariance of different times with a transition error; (c) updating the observation covariance based on analysis of the observation error; (d) update the truncation time based on the difference between previous and updated trajectory.

A. Updating the trajectory with sparse MAP

Setting ξ_T be the truncation time, $\mathcal{S}_k = \{\mathbf{s}_1, \dots, \mathbf{s}_k\}$ be the trajectory of states at time k , $\mathcal{Z}_k = \{\mathbf{Z}_1, \dots, \mathbf{Z}_k\}$ be the set of observations from time 1 to time k , the updated trajectory under optimization framework satisfies

$$\mathcal{S}_k^{(\xi_T:k)} = \arg \max P(\mathcal{S}_k^{(\xi_T:k)} | \mathcal{S}_{k-1}, \mathcal{Z}_k) \quad (34)$$

where $\mathcal{S}_k^{(\xi_T:k)} \subseteq \mathcal{S}_k$ is the part of trajectory during time $[\xi_T, k]$.

Assuming the observers are independent of each other, the probability of trajectory is

$$P(\mathcal{S}_k | \mathcal{Z}_k) = P(\mathbf{s}_1) \prod_{j=1}^n \frac{P(\mathbf{z}_1^{(j)} | \mathbf{s}_1)}{P(\mathbf{z}_1^{(j)})} \left\{ \prod_{i=2}^k P(\mathbf{s}_i | \mathbf{s}_{i-1}) \prod_{j=1}^n \frac{P(\mathbf{z}_i^{(j)} | \mathbf{s}_i)}{P(\mathbf{z}_i^{(j)})} \right\} \quad (35)$$

Typically, the observable is the position of object. It is linear with the state:

$$\mathbf{z} = \mathbf{H}\mathbf{s} + \delta\mathbf{z} \quad (36)$$

where \mathbf{H} is the observation matrix, $\delta\mathbf{z}$ is the observation error temporary assumed to obey normal distribution $\mathcal{N}\{\mathbf{0}, \mathbf{R}\}$, where \mathbf{R} has been updated in previous estimation.

Assuming the state transition satisfies the PLS model (33), where transition matrix $\boldsymbol{\Phi}_{i,i+1}, i = 1, 2, \dots, k-1$ is calculated by (29) based on the previous trajectory \mathcal{S}_{k-1} , the conditional probabilities in (35) satisfies:

$$\begin{cases} \log P(\mathbf{s}_i | \mathbf{s}_{i-1}) = -\frac{1}{2} \|\boldsymbol{\Phi}_{i-1,i} \mathbf{s}_{i-1} - \mathbf{s}_i\|_{\mathbf{Q}_{i-1,i}}^2 \\ \log P(\mathbf{z}_i^{(j)} | \mathbf{s}_i) = -\frac{1}{2} \|\mathbf{H}\mathbf{s}_i - \mathbf{z}_i^{(j)}\|_{\mathbf{R}_{i,j}}^2 \end{cases} \quad (37)$$

According to (35) and (37), the optimal trajectory of (34) satisfies the sparse linear equations

$$\mathcal{M}_k^{(\xi_T:k)} \mathcal{S}_k^{(\xi_T:k)} = \mathcal{B}_k^{(\xi_T:k)} \quad (38)$$

where $\mathcal{M}_k^{(\xi_T:k)} = \{\mathbf{M}_{i,j}, i, j = \xi_T, \dots, k\}$ is a sparse Matrix, and the nonzero elements satisfies:

$$\mathbf{M}_{i,i} = \begin{cases} \mathbf{H}^T \sum_{j=1}^n \mathbf{R}_{i,j}^{-1} \mathbf{H} + \boldsymbol{\Phi}_{i,i+1}^T \mathbf{Q}_{i,i+1}^{-1} \boldsymbol{\Phi}_{i,i+1} + \mathbf{Q}_{i-1,i}^{-1}, & i = \xi_T, \dots, k-1 \\ \mathbf{H}^T \sum_{j=1}^n \mathbf{R}_{k,j}^{-1} \mathbf{H} + \mathbf{Q}_{k-1,k}^{-1}, & i = k \end{cases} \quad (39)$$

$$\mathbf{M}_{i,i-1} = \mathbf{M}_{i-1,i}^T = \mathbf{Q}_{i-1,i}^{-1} \boldsymbol{\Phi}_{i-1,i}, \quad i = \xi_T + 1, \dots, k \quad (40)$$

$\mathcal{B}_k^{(\xi_T:k)} = \{\mathbf{b}_i, i = \xi_T, \dots, k\}$ is the set of vectors, the elements are:

$$\mathbf{b}_i = \begin{cases} \mathbf{H}^T \sum_{j=1}^n \mathbf{R}_{i,j}^{-1} \mathbf{z}_1^{(j)} + \mathbf{Q}_{i-1,i}^{-1} \boldsymbol{\Phi}_{i-1,i} \mathbf{x}_{i-1}, & i = \xi_T \\ \mathbf{H}^T \sum_{j=1}^m \mathbf{R}_{i,j}^{-1} \mathbf{z}_i^{(j)}, & i = \xi_T + 1, \dots, k \end{cases} \quad (41)$$

It should be noted that the set $\mathcal{M}_k^{(\xi_T:k)}$ can be expressed as a band-diagonal symmetric matrix, so equation (38) can be rapidly solved.

B. Adaptation of transition covariance

As a maneuvering object, it is hard to get an accurate prior statistics. This will lead to the extra error of the algorithms which urgently relying on the prior statistics. While the PLS is a nonlinear model, the error may be magnified. To be insensitive to the prior statistics, the transition covariance can be updated by a fading memory strategy,

$$\mathbf{Q}_{i,i+1} := \frac{t_m \mathbf{Q}_{i,i+1} + \tau \boldsymbol{\varepsilon}_{i,i+1}^{(k+1)} [\boldsymbol{\varepsilon}_{i,i+1}^{(k+1)}]^T}{t_m + \tau}, \quad i = 1, 2, \dots, k-1 \quad (42)$$

where $\mathbf{Q}_{i,i+1}$ is the transition covariance, respectively, and t_m is an empirical hyper-parameter of the memory time. $\boldsymbol{\varepsilon}_{i,i+1}^{(k+1)}$ is the transition error defined as:

$$\boldsymbol{\varepsilon}_{i,i+1}^{(k+1)} = \mathbf{s}_{i+1}^{(k+1)} - \boldsymbol{\Phi}_{k,k+1} \mathbf{s}_i^{(k+1)}, \quad i = 1, 2, \dots, k-1 \quad (43)$$

where $\mathbf{s}_i^{(k+1)}$ and $\mathbf{s}_{i+1}^{(k+1)}$ are the MAP of trajectory at time $k+1$.

Experiments show that after updating the state transition covariances, the overestimated part of the trajectory in a maneuver can be revised, which verified the improvement of the robustness to the biased prior statistics.

C. Adaptation of observation covariance

In most of the observation models, the prior statistics indicate that the noise of observation is zero-mean while it has drift in fact. This will lead to the systematic deviation of estimation. To solve the problem, we use an adaptation strategy to correct the covariance of abnormal observations based on the difference between the real observation and the estimated one from trajectory.

First, we define the observation bias as:

$$\delta \mathbf{z}_i^{(j)} = \mathbf{z}_i^{(j)} - \mathbf{H} \mathbf{s}_i \quad (44)$$

And the corresponding deviation:

$$e_z(\mathbf{z}_i^{(j)}) = \|\delta \mathbf{z}_i^{(j)}\|_{\mathbf{R}_{i,j}^{-1}} \quad (45)$$

where $\mathbf{z}_i^{(j)}$ is the real observation, $\mathbf{H} \mathbf{s}_i$ is the estimated observation from trajectory.

Then, the observation whose deviation is greater than 3 times of their RMSE will be considered as abnormal observation, and its covariance will be corrected with

$$\mathbf{R}_{i,j} = \frac{t_m \mathbf{R}_{i,j} + \tau \delta \mathbf{z}_i^{(j)} \delta \mathbf{z}_i^{(j)T}}{t_m + \tau} \quad (46)$$

Note that under the optimization framework with multiple sensors, (46) corrects not only the covariance of significantly deviated observations but also the covariance of drift observations. Compared with the classical filtering methods, it effectively avoids the negative effect of drift.

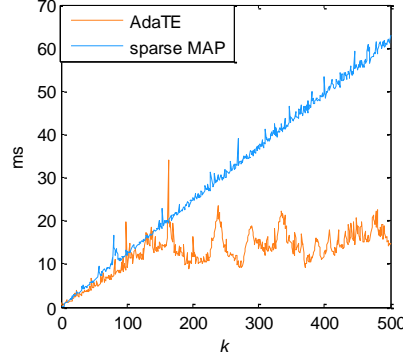


Fig 2. The time consumption of AdaTE and naive sparse MAP. The time consumption of sparse MAP linearly increases with the number of observations, while the time consumption of AdaTE fluctuates around 15 ms (the η is set to 0.000001).

D. Truncation time

While the trajectory only has regional correlations, the correlation between the observation and the state is inverse to the time interval. This means the latest observations will not influence the early states. In another word, in many situations the early states do not need to be updated. Based on this phenomenon, we defined a truncation time to limit the range of trajectory to be updated. It avoids the linear improvement of calculation in trajectory estimation.

The truncation index is defined as a weighted norm of the vector of difference between the same states in neighboring time:

$$\theta_i^{(k)} = \left\| s_i^{(k)} - s_i^{(k-1)} \right\|_{\psi}, i = 2, 3, \dots, k \quad (47)$$

where $s_i^{(k)}$ and $s_i^{(k-1)}$ are the i -th state of the trajectory estimated at time k and time $k-1$, and ψ is a diagonal weight matrix for each dimension of s .

Then the truncation time is defined as the latest time that all the truncation index before is smaller than threshold.

$$\xi_T = \max_i \left\{ \forall \theta_i^{(k)} < \eta, i = 1, \dots, t \right\} \quad (48)$$

where η is the threshold of truncation index.

If $\xi_T > 0$, the part of trajectory before it will be frozen, and only the part after it will be updated. To reserve sufficient information for the trajectory estimation, the truncation time is bounded by $\xi_T \leq k - 10$.

E. Adaptive trajectory estimation algorithm

Summarizing the above steps, the procedures of adaptive trajectory estimation is achieved in Algorithm.

To analyze the real-time performance of AdaTE, we compare the time consumptions of AdaTE algorithm with a naive sparse MAP algorithm [14] in a dataset containing 600 observations. Fig 2 shows the time consumption of the two algorithms for trajectory estimation. The result is obvious: compared with the sparse MAP, the AdaTE successfully limits the time consumption.

Algorithm: Adaptive trajectory estimation

Input: Previous estimation \mathcal{S}_{k-1} ; parameters $\xi_T, D_A, D_T, \mathcal{Q}_{i-1,i}$,

$\mathbf{R}_{i,j}, i \in \{1, \dots, k-1\}; \mathbf{Z}_i, i \in \{1, \dots, k\}$.

- Update transition matrices $\Phi_{i-1,i}, i \in \{\xi_T, \dots, k\}$ with (29).
 - Calculate the last transition covariance $\mathcal{Q}_{k-1,k}$ with (31).
 - Calculate the coefficients $\mathcal{M}_k^{(\xi_T:k)}$ and $\mathcal{B}_k^{(\xi_T:k)}$ from (39) to (41).
 - Update the part of trajectory $\mathcal{S}_k^{(\xi_T:k)}$ through sparse MAP (38); then combining with the previous part $\mathcal{S}_k = \{\mathcal{S}_{k-1}^{(1:\xi_T-1)}, \mathcal{S}_k^{(\xi_T:k)}\}$.
 - FOR $i \in \{\xi_T, \dots, k-1\}$
-

-
- Update the transition covariances $\mathbf{Q}_{i-1,i}$,
 $i \in \{\xi_T, \dots, k-1\}$ with (42).
 - Update the observation covariances $\mathbf{R}_{i,j}$ with (45) and
(46).
 - END
 - Update the truncation time ξ_T through (48)
-

Output: Updated trajectory \mathcal{S}_k ; parameters and statistics ξ_T ,

$\mathbf{Q}_{i-1,i}, \mathbf{R}_{i,j}; i \in \{1, \dots, k\}$

V. EXPERIMENTS

To evaluation the performance of AdaTE algorithm, we conducted three experiments: (a) typical trajectory estimation on 3D observations, (b) 3D path planning based on key points, and (c) trajectory optimization for visual tracking. The experiments were performed on a laptop with a 2.5GHz Intel Core i5 CPU with Matlab code.

A. Typical trajectory estimation on 3D observations

We test the AdaTE on three standard 3D trajectories with different characteristics, where the first one is a simple cruising route with minimal maneuvers; the second one is a swaying route with frequent variations of speed; the third one is a snake-like route with multiple maneuvers and some missing observations (from time 450 to 550). For each standard trajectory, there are two groups of observations: one produced with Gaussian noise and the other with additional drift.

In this experiment, all the prior statistics, including the transition covariance and the observation covariances are biased. And the contrast algorithms are EKF, UKF and sparse MAP. For the EKF and UKF, there are two different results with the constant acceleration model (CA) and PLS model. For sparse MAP, the dynamic model is constant turning (CT) model. The error is

measured with the normalized RMSE defined as $\frac{\text{RMSE}_{\text{result}}}{\text{RMSE}_{\text{observation}}}$.

The observations and the corresponding results of AdaTE are shown in Fig 3, where the figures on the first row show the observations under different conditions, and the figures on the second row are the estimated trajectory corresponding to the observations above. And in Fig 3 (b), (d), (f), parts of the observations have drifted. It should be noted that the AdaTE produces smooth and accurate estimation in all of the listed situations, even in the situation where both of the missing observation and observation drift occurs such as in group (f).

The normalized RMSE of each algorithm in experimental group (a)-(f) is presented in Fig 4. Compared with the contrasting algorithms, the AdaTE achieved the lowest mean normalized RMSE in all groups. Clearly, the EKF-PLS is divergent in all groups. The reason for the divergence is the linearization error of the strongly nonlinear PLS model and the biased prior statistics. Unexpectedly, in most groups, the result of the UKF with PLS model suffers a higher RMSE compared with the UKF with CA model. The reason might be the biased hypothesis that the transition error obeys a normal distribution, and the sigma sampling process magnifies this deviation. In contrast, the adaptation strategy drives the AdaTE substantially insensitive to the

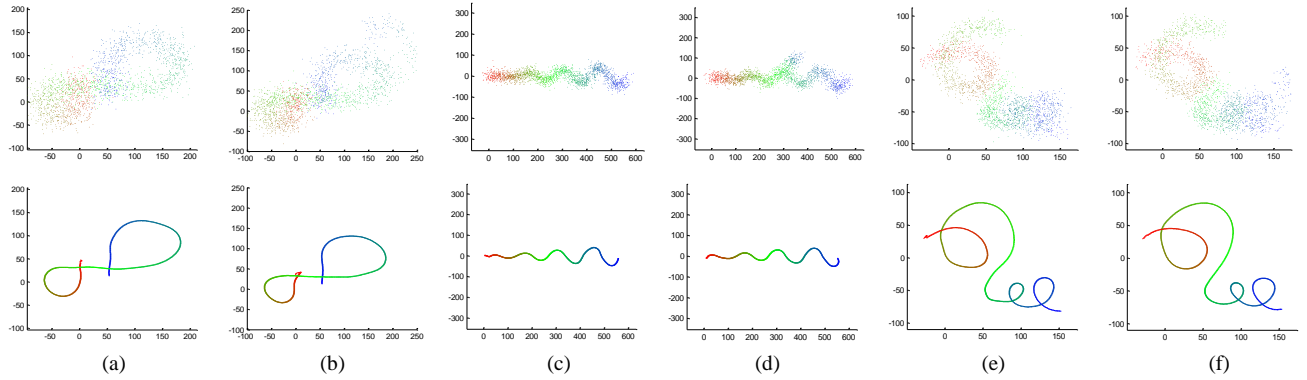


Fig 3. The observations and results of AdaTE in each group of experiments. The figures on the first row show the observations under different conditions, while the second row are the results corresponding to the observations above. The coloring from red to blue is consistent with the time order. Groups (a) and (b) are based on cruising route, groups (c) and (d) are based on a swaying route, and groups (e) and (f) are based on a snake-like route with missing observations. Observation drift is added to (b), (d) and (f)

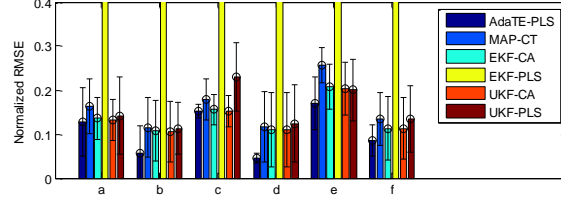


Fig 4. The normalized RMSE of algorithms in each group of experiments, where (a)-(f) is the order of experiments. The bars represent the mean normalized RMSE of each algorithm, while the error lines represent the range decided by standard deviations. Note that the EKF-PLS has a divergent result in each group, and the normalized RMSE is beyond the range of the table.

biased prior statistics and robust to the observation drift and missing. The detail for the mean normalized RMSE in each group of experiments can be found in Table I.

TABLE I
STATISTICS OF THE RMSE IN THE TRAJECTORY ESTIMATION TASK

	Cruise		Swaying		Snake-like	
Observation drift	no	yes	no	yes	no	yes
AdaTE-PLS	0.128	0.056	0.152	0.045	0.169	0.086
MAP-CT	0.164	0.115	0.179	0.117	0.257	0.135
EKF-CA	0.136	0.107	0.156	0.110	0.208	0.113
EKF-PLS	Div	Div	Div	Div	Div	Div
UKF-CA	0.133	0.106	0.152	0.110	0.204	0.113
UKF-PLS	0.142	0.113	0.230	0.124	0.201	0.135
Observation RMSE	24.784	58.889	23.647	91.253	14.186	28.024

The error used to evaluate the algorithms is the mean normalized RMSE. The observation RMSE in each group is given as the absolute value. The bold number in each group is the smallest mean normalized RMSE, and Div denotes that the normalized RMSE is invalid for the divergence. AdaTE-PLS obtains the minimum error in all groups.

B. 3D Path planning based on key points

The key points based path planning is commonly applied in large scale navigation [38][39]. Based on the topological map, the shortest (or optimal) path between any two nodes can be rapidly found out. After the planning on topological level, sometimes we want to find out the path with least control between adjacent nodes to save the energy. This is exactly a suitable task for AdaTE.

In this scenario, the object has to avoid the moving obstacles while finding a best trajectory online. Based on this requirement, we design a strategy where the object only considers into two upcoming nodes in path planning so it could response more flexible to the obstacles.

Setting \mathbf{P} be the set of nodes, $\mathbf{\Omega}$ be the set of obstacles, and t_k be the time of arrival at upcoming node, the MAP of the planned path can be described as

$$\mathbf{S}_k^{(k:t_k)} = \arg \max_{\mathbf{X}_k^{(k:t_k)}} \mathcal{L}(\mathbf{S}_k^{(k:t_k)}; \mathbf{S}_{k-1}^{(k:t_{k-1})}, \mathbf{P}, \mathbf{\Omega}) \quad (49)$$

where

$$\begin{aligned} \mathcal{L}(\mathbf{S}_k^{(k:t_k)}; \mathbf{S}_{k-1}^{(k:t_{k-1})}, \mathbf{P}, \mathbf{\Omega}) = \\ \log P(\mathbf{S}_k^{(k:t_k)} | \mathbf{S}_{k-1}^{(k:t_{k-1})}) + \log P(\mathbf{P} | \mathbf{S}_k^{(k:t_k)}) + \\ \log P_a(\mathbf{\Omega} | \mathbf{S}_k^{(k:t_k)}) \end{aligned} \quad (50)$$

and

$$P_a(\mathbf{\Omega} | \mathbf{S}_k^{(k:t_k)}) = \prod_{i=k}^{t_k} (1 - P_h(\mathbf{\Omega} | \mathbf{S}_k^{(i)})) \quad (51)$$

where $P_a(\mathbf{\Omega} | \mathbf{S}_k^{(k:t_k)})$ is the unblocked probability of the planned path and $P_h(\mathbf{\Omega} | \mathbf{S}_k^{(i)})$ is the unblocked probability at point i .

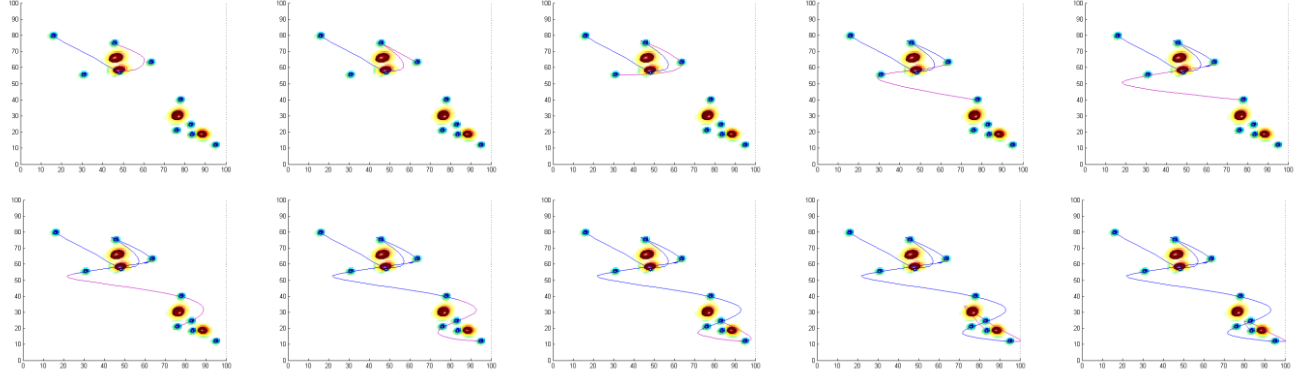


Fig 5. Overview of the 3D path planning based on key points at 10 representative moments. From left to right, the images on the top are overviews at times 10, 11, 21, 31, and 34. In addition, the bottom images are at times 41, 51, 61, 71, and 73. The dark blue ellipsoids are key points, and their radii in different direction represent the covariance; the sky blue region around the key points is the nearby region within two standard derivations. The dark red ellipsoids are the forbidden regions of the obstacles, while the yellow regions around them are the warning areas. The dark blue curve is the historical path, and the purple curve is the planned path.

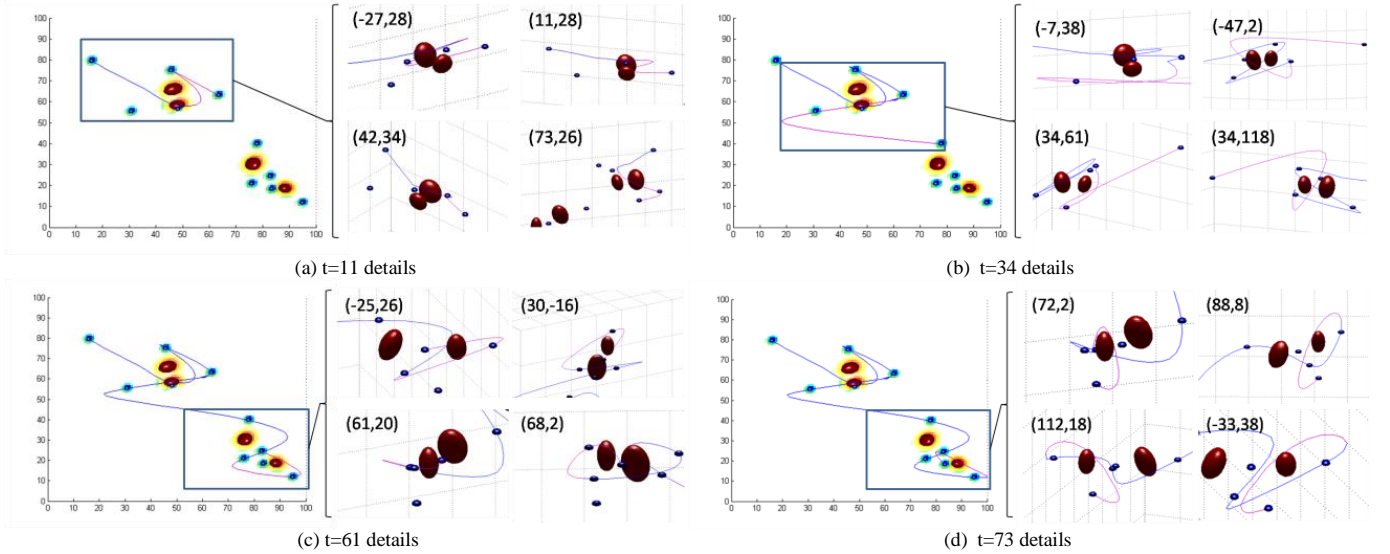


Fig 6. The regional details of obstacle avoidance at 4 representative moments, where subgraphs (a)-(d) correspond to times 11, 34, 61 and 73. Each subgraph shows partial details from 4 different views, where the corresponding viewing angle is indicated at the top left. The dark blue curve is the historical path, and the purple curve is the planned path.

Based on the maximum probability defined in (51), the optimal regional path could be solved by AdaTE. The dynamic path planning process is shown in Fig 5. We can observe the original plan is slightly adjusted when the object arrived at an upcoming node and a new upcoming node is taken into consideration (compare the pink curve at time 10 with that at time 11). Another detail is the plan at time 34 is adjusted based on the plan at time 31. This is because the original plan is failed to avoid the moving obstacle; therefore, it was fixed at time 34 to forbid the obstacle from its bottom (for details, please turn to Fig 6 (b)), thus extending the path and increasing the speed, leading to a larger radius of the turning circle. A similar situation occurred from times 71 to time 73.

The projections of the 3D path planning cannot show the details of the obstacle avoidance, especially when the path passes the obstacle from above or below, the object appearing to be intersecting them. To prevent a misunderstanding, some regional details of the obstacle avoidance at different moments are presented in Fig 6. In general, AdaTE uses minimum energy under the constraint of the dynamic model and the upcoming nodes to avoid the obstacles. In this experiment, the path converges in 3 loops of iterations for a single obstacle. And it needs no more than 4 iterations for two obstacles.

C. Trajectory optimization for visual tracking

To test the performance of AdaTE in visual tracking, we choose eight scenes in VOT 2013 with illumination variations

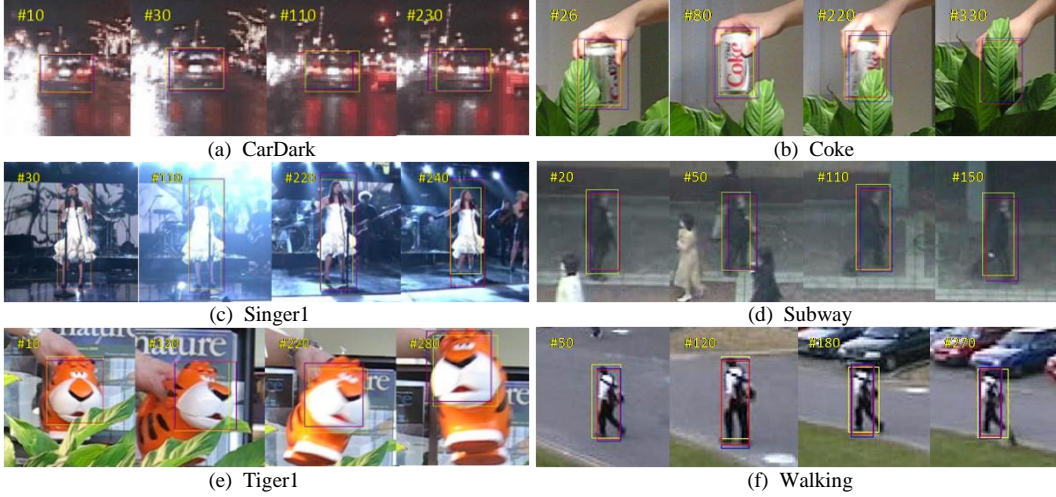


Fig 7. Some screenshots of visual tracking experiments, including the result of original fDSST (blue box), the result estimated by fDSST-AdaTE (red box), and the ground truth (yellow box). Note that in most of the images, the fDSST-AdaTE method obtained a slightly better result than fDSST.

(CarDark and Singer1), scale variations (Singer1) and partial blocking (Coke and Tiger1) for the experiment. The fDSST [21] is used as the basic tracking algorithm, and the mean overlap is chosen as the evaluation index. Parts of the screenshots are presented in Fig 7. It can be observed that in most samples, the AdaTE achieves a slight improvement in accuracy compared with basic fDSST.

The mean overlap of the experiment in each scene is shown in TABLE II. In most scenes, fDSST-AdaTE is superior to the basic fDSST with weak advantage. We find that as a model-based algorithm, AdaTE is robust to the shaky observations compared with the original tracking algorithm. However, AdaTE cannot distinguish small shakiness from noise with the shakiness in real motion, thus leading to the extra estimation error in certain scenes, such as the Coke and Tiger2. Compared with applying to a smooth tracking algorithm like DSST, AdaTE is likely to achieve a more obvious improvement for a wobbly tracking algorithm such as SAMF [22].

TABLE II
MEAN OVERLAP ON 8 SCENES FROM THE VOT 2013 DATASET

	fDSST	fDSST- AdaTE	Increase
<i>vot-cardark</i>	0.7422	0.7507	1.16%
<i>vot-coke</i>	0.5589	0.5604	0.27%
<i>vot-tiger1</i>	0.7337	0.7349	0.17%
<i>vot-tiger2</i>	0.6759	0.6723	-0.53%
<i>vot-walking</i>	0.7257	0.7333	1.05%
<i>vot-subway</i>	0.6880	0.6914	0.50%
<i>vot-singer1</i>	0.8042	0.8149	1.33%
<i>vot-dudek</i>	0.8034	0.8062	0.35%

A comparison of fDSST and fDSST-AdaTE in visual tracking task for 8 scenes from the VOT 2013 dataset. The mean overlap was chosen as the index to evaluate the algorithms. In most scenes, the fDSST-AdaTE has a better result compared with fDSST.

VI. CONCLUSION

In this paper, we investigate the online trajectory estimation with regional correlations under the condition of biased prior statistics and observations drift. To estimate the trajectory without the specific dynamic model of object, we learn from the previous works and propose the power-limited steering model (PLS), as well as deriving its corresponding form in discrete time. It is a natural combination of instantaneous power theory and instantaneous angular velocity theory from Newtonian mechanics. Compared with constant mean acceleration model, it overcomes the infinite velocity problem in prediction with the joint action of power and resistance. Compared with Markov process models, the strong nonlinearity make it only needs few prior parameters for describing the typical states.

To overcome the difficulties in trajectory estimation such as the biased prior statistics, the observations drift and linear growing computation, we propose the adaptive trajectory estimation Igorithm (AdaTE) based on the PLS model. During its four procedures, the sparse maximum a posterior estimation speeds up the solving process. The adaptation of transition covariance improves the robustness to both the model error and the prior statistics. The correction of observation covariance improves the resistance to the observation drift. And the truncation time ensures the update is confined to necessary part, which avoids the linear improvement of calculation.

To evaluate the performance of AdaTE-PLS in different tasks, we conduct three experiments: (a) extensive trajectory estimation, (b) 3D path planning based on key points, (c) trajectory optimization for visual tracking. In task (a), the AdaTE-PLS yields superior results compared with other methods under the biased statistics and drift observation. In task (b), the AdaTE-PLS uses minimum energy to avoid the obstacles under the soft constraints of the key points. In task (c), the AdaTE is proven to improve the precision of trajectory in most cases compared with basic tracking algorithm.

In the future, we will explore better general dynamic model which is simpler, less computation and more precise for maneuvering object. Furthermore, we hope to extend the AdaTE algorithm to a wider probability distribution, such as the exponential family, to develop a more significant and general optimization method.

APPENDIX A

SOLVING THE PREDICTED VELOCITY FROM PLS MODEL WHEN IGNORING PERTURBATION

When ignoring the perturbation of p in differential equation (15) during a short time $(t, t + \tau)$, the axial velocity satisfies:

$$\frac{|\mathbf{v}|}{\alpha |\mathbf{v}|^2 + \beta |\mathbf{v}| - p} d|\mathbf{v}| = -dt \quad (52)$$

where p has a fixed value during $(t, t + \tau)$.

Rewrite (52) as:

$$\left(\frac{\varsigma_1}{|\mathbf{v}| + \varsigma_1} - \frac{\varsigma_2}{|\mathbf{v}| + \varsigma_2} \right) d|\mathbf{v}| = -\gamma dt \quad (53)$$

where

$$\begin{cases} \varsigma_1 = \frac{\beta + \sqrt{\beta^2 + 4\alpha p^*}}{2\alpha} \\ \varsigma_2 = \frac{\beta - \sqrt{\beta^2 + 4\alpha p^*}}{2\alpha} \end{cases} \quad (54)$$

$$\gamma = \sqrt{\beta^2 + 4\alpha p} \quad (55)$$

The biased estimation of $|\mathbf{v}|$ can be solved from (53):

$$\left[\varsigma_1 \log(|\hat{\mathbf{v}}| + \varsigma_1) - \varsigma_2 \log(|\hat{\mathbf{v}}| + \varsigma_2) \right]_t^{t+\tau} = -\gamma\tau \quad (56)$$

Calculate the exponential on both side of (56), we get,

$$\left(\frac{|\hat{\mathbf{v}}(t + \tau)| + \varsigma_1}{|\mathbf{v}(t)| + \varsigma_1} \right)^{\varsigma_1} \left(\frac{|\hat{\mathbf{v}}(t + \tau)| + \varsigma_2}{|\mathbf{v}(t)| + \varsigma_2} \right)^{-\varsigma_2} = e^{-\gamma\tau} \quad (57)$$

Then consider the orientation of velocity. From (16) the orientation of velocity satisfies,

$$\frac{d}{dt} \frac{\mathbf{v}}{|\mathbf{v}|} = [\mathbf{c}_T]_{\times} \frac{\mathbf{v}}{|\mathbf{v}|} \quad (58)$$

Solving (58), we can get the orientation of velocity,

$$\frac{\hat{\mathbf{v}}(t + \tau)}{|\hat{\mathbf{v}}(t + \tau)|} = \exp\left(\tau [\mathbf{c}_T(t)]_{\times}\right) \frac{\mathbf{v}(t)}{|\mathbf{v}(t)|} \quad (59)$$

Combining (57) and (59) together, the relationship between previous velocity $|\mathbf{v}(t)|$ and predicted velocity $|\hat{\mathbf{v}}(t + \tau)|$ is,

$$\begin{cases} \left(\frac{|\hat{\mathbf{v}}(t + \tau)| + \varsigma_1}{|\mathbf{v}(t)| + \varsigma_1} \right)^{\varsigma_1} \left(\frac{|\hat{\mathbf{v}}(t + \tau)| + \varsigma_2}{|\mathbf{v}(t)| + \varsigma_2} \right)^{-\varsigma_2} = e^{-\gamma\tau} \\ \frac{\hat{\mathbf{v}}(t + \tau)}{|\hat{\mathbf{v}}(t + \tau)|} = \exp\left(\tau [\mathbf{c}_T(t)]_{\times}\right) \frac{\mathbf{v}(t)}{|\mathbf{v}(t)|} \end{cases} \quad (60)$$

APPENDIX B

THE COMPENSATION OF VELOCITY BASED ON THE RENORMALIZATION GROUP

Setting the axial velocity $v = |\mathbf{v}|$. From (15), the function of axial acceleration is,

$$a_{A0}(v) = \frac{p}{v} - \alpha v - \beta \quad (61)$$

At reference time t , the zero order axial velocity is $v_0 = |\mathbf{v}(t)|$, from (61) the first order renormalization of v satisfies,

$$v_1(t+\tau) = v_0 + \int_t^{t+\tau} a_A(v_0) ds = v_0 + \frac{\tau p(t) + r^{(1)}(\tau)}{v_0} - \tau(\alpha v_0 + \beta) \quad (62)$$

where $r^{(1)}(\tau) = \int_0^\tau \int_0^s u_A(t) ds dt$ obeys $\mathcal{N}\left\{0, \frac{1}{3}\tau^3 D_A\right\}$.

Put v_1 into (61) we can get $a_{A0}(v_1)$. Then plug $a_{A0}(v_1)$ into (62), we will obtain the second order renormalization of v ,

$$\begin{aligned} v_2(t+\tau) &= v_0 + \int_t^{t+\tau} a_A(v_1) ds \\ &= v_0 + \int_0^\tau \frac{p(t) + r(s)}{v_0 + \frac{sp(t) + r^{(1)}(s)}{v_0} - s(\alpha v_0 + \beta)} ds + \Omega(t+\tau) \end{aligned} \quad (63)$$

where $r(s) = \int_0^s u_A(t) dt$ obeys $\mathcal{N}\{0, \tau D_A\}$

Noticing that when τ is a small number, and $v_0 \neq 0 \vee p(t) \neq 0$, (63) can be rewritten as,

$$\begin{aligned} v_2(t+\tau) &= \\ &= \int_0^\tau \frac{v_0(p(t) + r(s)) \left[v_0^2 + sp(t) - sv_0(\alpha v_0 + \beta) - r^{(1)}(s) \right]}{\left(v_0^2 + sp(t) - sv_0(\alpha v_0 + \beta) \right)^2 - \left[r^{(1)}(s) \right]^2} ds + \Omega(t+\tau) \\ &\approx - \int_0^\tau \frac{v_0 r(s) r^{(1)}(s)}{\left(v_0^2 + sp(t) - sv_0(\alpha v_0 + \beta) \right)^2} ds + \Omega(t+\tau) \end{aligned} \quad (64)$$

Where $\Omega(t+\tau)$ is the part of velocity ignoring disturbance, which is equal to $|\hat{\mathbf{v}}(t+\tau)|$ in this paper.

Based on (64), the expectation of $v_2(t+\tau)$ is,

$$\begin{aligned} E[v_2(t+\tau)] &\approx -v_0 \int_0^\tau \frac{E[r(s)r^{(1)}(s)]}{\left(v_0^2 + sp(t) - sv_0(\alpha v_0 + \beta) \right)^2} ds + \Omega(t+\tau) \\ &= \Delta v(t, t+\tau) + \Omega(t+\tau) \end{aligned} \quad (65)$$

where

$$E[r(s)r^{(1)}(s)] = E\left[\int_0^s \int_0^\rho u_A(t) dt d\rho \cdot \int_0^s u_A(t) dt \right] = \frac{1}{2} s^2 D_A \quad (66)$$

and $\Delta v(t, t+\tau)$ is the compensation part of $E[v(t+\tau)]$,

$$\begin{aligned} \Delta v(t, t+\tau) &= \\ &= -\frac{v_0 D_A}{2\mu(t)} \left[\tau - \frac{2v_0^2}{\mu(t)} \log \frac{v_0^2 + \tau\mu(t)}{v_0^2} + \frac{v_0^2 \tau}{v_0^2 + \tau\mu(t)} \right] \end{aligned} \quad (67)$$

where $\mu(t) = p(t) - v_0(\alpha v_0 + \beta)$.

From (16), the angular velocity $\frac{d}{dt} \frac{\mathbf{v}}{|\mathbf{v}|}$ is linear with $\frac{\mathbf{v}}{|\mathbf{v}|}$ and $[\mathbf{c}_T]_\times$, so the \mathbf{u}_T will not act on the expectation of orientation, it doesn't need any compensation.

APPENDIX C

THE APPROXIMATED PRIMARY VALUE OF TRANSITION COVARIANCE

From (31) the transition covariance satisfies,

$$\mathbf{Q}(t, t + \tau) = \int_t^{t+\tau} \mathbf{\Phi}(t, s) \mathbf{D}_u \mathbf{\Phi}^T(t, s) ds \quad (68)$$

where \mathbf{D}_u satisfies (32)

Substituting (29) into (68), the transition covariance will be,

$$\mathbf{Q}(t, t + \tau) = \begin{bmatrix} \Sigma_{11}(t, t + \tau) & \Sigma_{12}(t, t + \tau) & \Sigma_{13}(t, t + \tau) & \Sigma_{14}(t, t + \tau) \\ \Sigma_{12}^T(t, t + \tau) & \Sigma_{22}(t, t + \tau) & \Sigma_{23}(t, t + \tau) & \Sigma_{24}(t, t + \tau) \\ \Sigma_{13}^T(t, t + \tau) & \Sigma_{23}^T(t, t + \tau) & \Sigma_{33}(t, t + \tau) & \mathbf{0} \\ \Sigma_{14}^T(t, t + \tau) & \Sigma_{24}^T(t, t + \tau) & \mathbf{0} & \Sigma_{44}(t, t + \tau) \end{bmatrix} \quad (69)$$

Where

$$\begin{cases} \Sigma_{11}(t, t + \tau) = \int_t^{t+\tau} D_A \mathbf{\Phi}_{13}(t, s) \mathbf{\Phi}_{13}^T(t, s) + \mathbf{\Phi}_{14}(t, s) D_T \mathbf{\Phi}_{14}^T(t, s) ds \\ \Sigma_{12}(t, t + \tau) = \int_t^{t+\tau} D_A \mathbf{\Phi}_{13}(t, s) \mathbf{\Phi}_{23}^T(t, s) + \mathbf{\Phi}_{14}(t, s) D_T \mathbf{\Phi}_{24}^T(t, s) ds \\ \Sigma_{13}(t, t + \tau) = \int_t^{t+\tau} D_A \mathbf{\Phi}_{13}(t, s) ds \\ \Sigma_{14}(t, t + \tau) = \int_t^{t+\tau} \mathbf{\Phi}_{14}(t, s) D_T ds \end{cases} \quad (70)$$

and

$$\begin{cases} \Sigma_{22}(t, t + \tau) = \int_t^{t+\tau} D_A \mathbf{\Phi}_{23}(t, s) \mathbf{\Phi}_{23}^T(t, s) + \mathbf{\Phi}_{24}(t, s) D_T \mathbf{\Phi}_{24}^T(t, s) ds \\ \Sigma_{23}(t, t + \tau) = \int_t^{t+\tau} D_A \mathbf{\Phi}_{23}(t, s) ds \\ \Sigma_{24}(t, t + \tau) = \int_t^{t+\tau} \mathbf{\Phi}_{24}(t, s) D_T ds \end{cases} \quad (71)$$

and

$$\begin{cases} \Sigma_{33}(t, t + \tau) = \tau D_A \\ \Sigma_{44}(t, t + \tau) = \tau D_T \end{cases} \quad (72)$$

Ignoring the high order quantity about τ , the approximation of each submatrix is,

$$\begin{cases} \Sigma_{11}(t, t + \tau) \approx \frac{\tau^3}{12} D_A \left(1 - e^{-\lambda \tau} g_{(t, t+\tau)}\right)^2 \frac{h_{(t, t+\tau)}^2}{|\mathbf{v}(t)|^2} \mathbf{v}(t) \mathbf{v}(t)^T - \frac{1}{20} \tau^5 \varphi_{(t, t+\tau)}^2 [\mathbf{v}(t)]_{\times} D_T [\mathbf{v}(t)] \\ \Sigma_{12}(t, t + \tau) \approx \frac{\tau^2}{4} D_A (1 - e^{-\lambda \tau} g_{(t, t+\tau)})^2 \frac{h_{(t, t+\tau)}^2}{|\mathbf{v}(t)|^2} \mathbf{v}(t) \mathbf{v}(t)^T - \frac{1}{8} \tau^4 \varphi_{(t, t+\tau)}^2 [\mathbf{v}(t)]_{\times} D_T [\mathbf{v}(t)] \\ \Sigma_{13}(t, t + \tau) = \frac{\tau^2}{4} D_A g_{(t, t+\tau)} \frac{h_{(t, t+\tau)}}{|\mathbf{v}(t)|} \mathbf{v}(t) \\ \Sigma_{14}(t, t + \tau) = -\frac{1}{6} \tau^3 \varphi_{(t, t+\tau)} [\mathbf{v}(t)]_{\times} D_T \end{cases} \quad (73)$$

and

$$\begin{cases} \Sigma_{22}(t, t+\tau) = \tau D_A (1 - g_{(t,t+\tau)})^2 \frac{h_{(t,t+\tau)}^2}{|v(t)|^2} v(t) v(t)^T - \frac{1}{3} \tau^3 \varphi_{(t,t+\tau)}^2 [v_k]_{\times} D_T [v_k] \\ \Sigma_{23}(t, t+\tau) = \tau D_A g_{(t,t+\tau)} \frac{h_{(t,t+\tau)}}{|v(t)|} v(t) \\ \Sigma_{24}(t, t+\tau) = -\frac{1}{2} \tau^2 \varphi_{(t,t+\tau)} [v(t)]_{\times} D_T \end{cases} \quad (74)$$

REFERENCES

- [1] E.A. Wan, and R. Van Der Merwe. "The unscented Kalman filter for nonlinear estimation." IEEE Adaptive Systems for Signal Processing, Communications, and Control Symposium. Alberta, Canada, 2000, pp. 153–158.
- [2] Merwe, R. Van Der, and E. A. Wan. "The square-root unscented Kalman filter for state and parameter-estimation." IEEE International Conference on Acoustics, Speech, and Signal Processing, 2001. Proceedings IEEE, 2002:3461-3464 vol.6.
- [3] Grisetti, G., Kummerle, R., Stachniss, C., & Burgard, W. (2011). "A tutorial on graph-based slam." IEEE Intelligent Transportation Systems Magazine, 2(4), 31-43.
- [4] Kummerle R, Grisetti G, Strasdat H, et al. "G2o: A general framework for graph optimization." IEEE International Conference on Robotics and Automation. IEEE, 2011:3607-3613.
- [5] Li, X. Rong, and V. P. Jilkov. "Survey of maneuvering target tracking. Part I. Dynamic models." IEEE Transactions on Aerospace & Electronic Systems 39.4(2004):1333-1364.
- [6] Bar-Shalom, Y., Li, X. R., and Kirubarajan, T. "Estimation with Applications to Tracking and Navigation: Theory, Algorithms, and Software." New York: Wiley, 2001.
- [7] Singer, R. A. "Estimating optimal tracking filter performance for manned maneuvering targets." Transactions on Aerospace and Electronic Systems, AES-6. 1970, 473–483.
- [8] Campo, L., Mookerjee, P., and Bar-Shalom Y.. "State estimation for systems with sojourn-time-dependent Markov model switching." IEEE Transactions on Automatic Control 36.2(1991):238-243.
- [9] Berg, R. F. . "Estimation and prediction for maneuvering target trajectories." IEEE Transactions on Automatic Control 28.3(1983):294-304.
- [10] Fan, X., Fan G., and J. P. Havlicek. "Generative Model for Maneuvering Target Tracking." IEEE Transactions on Aerospace & Electronic Systems 46.2(2010):635-655.
- [11] Maybeck, P. S., Worsley, W. H., and Flynn, P. M. (1982) Investigation of constant turn-rate dynamics for airborne vehicle tracking. In Proceedings of the National Aerospace and Electronics Conference (NAECON), 1982, 896–903.
- [12] Bryan, R. S. (1980) Cooperative estimation of targets by multiple aircraft. M.S. thesis, Air Force Institute of Technology, Wright-Patterson AFB, Ohio, June, 1980.
- [13] RAUCH, et al. "Maximum likelihood estimates of linear dynamic systems." Aiaa Student Journal American Institute of Aeronautics & Astronautics 3 i8.3 i8(2012):1445-1450.
- [14] W. Li, X. Yang, C. He, S. Ren and Y. Zhang, "Online maximum likelihood filtering for aircraft tracking under low accuracy observations," 2017 Chinese Automation Congress (CAC), Jinan, 2017, pp. 1998-2005.
- [15] Xinyan Yan, VadimIndelman, and Byron Boots. "Incremental Sparse GP Regression for Continuous-Time Trajectory Estimation and Mapping." Robotics and Autonomous Systems 87(2017):120-132.
- [16] Mercieca, J. P. Aram, and V. Kadiramanathan. "Unscented Rauch-Tung-Striebel smoothing for nonlinear descriptor systems." Control Conference IEEE, 2015:491-496.
- [17] KatjaNummiaro, Esther Koller-Meier, and Luc Van Gool. "An adaptive color-based particle filter." Image and Vision Computing 21.1(2003):99-110.
- [18] Zhang, Tianzhu, C. Xu, and M. H. Yang. "Multi-task Correlation Particle Filter for Robust Object Tracking." IEEE Conference on Computer Vision and Pattern Recognition IEEE Computer Society, 2017:4819-4827.
- [19] Hol, Jeroen D., T. B. Schon, and F. Gustafsson. "On Resampling Algorithms for Particle Filters." IEEE Nonlinear Statistical Signal Processing Workshop IEEE, 2007:79-82.
- [20] Moral, P. Del. "Nonlinear filtering: Interacting particle solution." Markov Processes & Related Fields 2.4(1996):555-580.
- [21] Danelljan, Martin, et al. "Discriminative Scale Space Tracking." IEEE Transactions on Pattern Analysis & Machine Intelligence 39.8(2017):1561-1575.
- [22] Li Y, Zhu J. "A Scale Adaptive Kernel Correlation Filter Tracker with Feature Integration". IEEE European Conference on Computer Vision 2014, 8926:254-265.
- [23] Arasaratnam, Ienkaran, and S. Haykin. "Cubature Kalman Filters." IEEE Transactions on Automatic Control 54.6(2009):1254-1269.
- [24] Nguyen, Trung, et al. "Developing a Cubature Multi-state Constraint Kalman Filter for Visual-Inertial Navigation System." Conference on Computer and Robot Vision IEEE Computer Society, 2017:321-328.
- [25] Johansen, Tor A., and T. I. Fossen. "The eXogenous Kalman Filter (XKF)." International Journal of Control 90.2(2017):161-167.
- [26] Chen, Badong, et al. "Maximum correntropy Kalman filter." Automatica 76(2017):70-77.
- [27] M. Zorzi, "Robust Kalman Filtering Under Model Perturbations," in IEEE Transactions on Automatic Control, vol. 62, no. 6, pp. 2902-2907, June 2017
- [28] Carlone, Luca, et al. "Planar Pose Graph Optimization: Duality, Optimal Solutions, and Verification." IEEE Transactions on Robotics 32.3(2016):545-565.
- [29] F. Lu, and E. Milios. "Globally Consistent Range Scan Alignment for Environment Mapping." Autonomous Robots 4.4(1997):333-349.
- [30] Kaess, Michael. "Incremental smoothing and mapping." IEEE Transactions on Robotics 24.6(2008):1365-1378.
- [31] Hwang, Joo Young, et al. "A fast path planning by path graph optimization." Systems Man & Cybernetics Part A Systems & Humans IEEE Transactions on 33.1(2003):121-129.
- [32] Davison, Andrew J, et al. "MonoSLAM: Real-Time Single Camera SLAM." IEEE Transactions on Pattern Analysis and Machine Intelligence 29.6(2007):1052-1067.
- [33] Engel, Jakob, T. Schöps, and D. Cremers. "LSD-SLAM: Large-Scale Direct Monocular SLAM." European Conference on Computer

- Vision 8690(2014):834-849.
- [34] Mur-Artal, Raúl, J. M. M. Montiel, and J. D. Tardós. "ORB-SLAM: A Versatile and Accurate Monocular SLAM System." *IEEE Transactions on Robotics* 31.5(2017):1147-1163.
 - [35] Liu, D. C, and J. Nocedal. "On the limited memory BFGS method for large scale optimization." *Mathematical Programming* 45.1-3(1989):503-528.
 - [36] Mandic, D. P. "A generalized normalized gradient descent algorithm." *Signal Processing Letters IEEE* 11.2(2004):115-118.
 - [37] Zwanzig, Robert. "Nonequilibrium statistical mechanics." Oxford University Press, 2001.
 - [38] Bortoff S A. "Path planning for UAVs." *Proceedings of the 2000 American Control Conference. ACC (IEEE Cat. No. 00CH36334)*. IEEE, 2000, 1(6): 364-368.
 - [39] Li Y, Park J H, Shin B S. "A shortest path planning algorithm for cloud computing environment based on multi-access point topology analysis for complex indoor spaces". *The Journal of Supercomputing*, 2017, 73(7): 2867-2880.